American Mineralogist, Volume 92, pages 460–467, 2007

Hammadah al Hamra 193: The first amphibole-bearing winonaite

Christine Floss,[1,*] Bradley L. Jolliff,[2] Gretchen K. Benedix,[2,3] Frank J. Stadermann,[1] and Jay Reid[2]

[1]Laboratory for Space Sciences and Physics Department, Washington University, One Brookings Drive, St. Louis, Missouri 63130, U.S.A.
[2]Department of Earth and Planetary Sciences, Washington University, One Brookings Drive, St. Louis, Missouri 63130, U.S.A.
[3]Department of Mineralogy, The Natural History Museum, Cromwell Road, London, SW7 5BD, U.K.

Abstract

The Hammadah al Hamra 193 winonaite was found in the Libyan desert in 1996. Unlike most winonaites with fine- to medium-grained equigranular textures, it consists predominantly of very large (up to 5 mm), optically continuous orthopyroxene grains enclosing smaller grains of olivine and plagioclase. It also contains large (up to 2 mm) poikilitic grains of amphibole enclosing clinopyroxene, plagioclase, olivine, and occasionally orthopyroxene, which occur interstitial to the large orthopyroxene grains. The amphibole is identified as fluoro-edenite, and textures indicate that it replaces clinopyroxene via a reaction in which diopside, olivine, and plagioclase form fluoro-edenite. Trace-element data are consistent with the formation of fluoro-edenite from clinopyroxene and plagioclase. Fluoro-edenite has a REE pattern similar to that of clinopyroxene, but has elevated abundances of Na, K, and Ba, elements typically enriched in plagioclase. The source of the F is uncertain, but may be apatite, which is fluor-apatite in this meteorite. The presence of fluoro-edenite in HaH 193, a meteorite that experienced extensive thermal metamorphism, indicates a significant stability field for this rare mineral.

Keywords: Meteorites, winonaites, amphibole, metamorphism

Introduction

The winonaites are a relatively small group (~17 known members) of reduced meteorites (i.e., iron is present as either Fe^0 or Fe^{2+}). Their oxygen isotopic compositions are distinct from those of other meteorite groups, except for silicate inclusions in IAB iron meteorites (Clayton and Mayeda 1996; Benedix et al. 1998), to which they are thought to be related (Benedix et al. 2000). The winonaites are primitive achondrites and typically exhibit chondritic mineral assemblages and bulk chemistries, but non-chondritic textures. Like other primitive achondrite groups (e.g., the acapulcoites and lodranites; McCoy et al. 1996, 1997; Floss 2000), they appear to have experienced extensive metamorphism and partial melting, but have escaped the complete differentiation characteristic of basaltic meteorites such as the eucrites. Winonaites thus have the potential to provide information about early heating processes in asteroidal bodies.

Benedix et al. (1998, 2000) carried out a systematic study of the winonaites and silicate inclusions in IAB iron meteorites, and concluded that these meteorites formed from heterogeneous chondritic precursor materials that experienced partial melting, impact brecciation, and extensive metamorphism. Most winonaites are fine- to medium-grained with equigranular, recrystallized textures, but several contain millimeter-sized areas that differ substantially in grain size and/or mineralogy from the surrounding matrix. Such areas include fine-grained plagioclase- and pyroxene-rich areas in Pontlyfni that may represent partial melts, coarse-grained olivine clumps in Winona and Mt. Morris that are interpreted as partial melt residues, and large poikilitic calcic pyroxenes enclosing smaller olivine, orthopyroxene, and plagioclase grains in Tierra Blanca (Benedix et al. 1998). Some winonaites, most notably NWA 1463, contain relict chondrules (Benedix et al. 2003), attesting to the chondritic origin of this meteorite group.

Hammadah al Hamra (HaH) 193 was found in the Libyan desert as a single stone of 259 g, and was identified as a winonaite on the basis of its mineral compositions (Grossman 1998). This classification was later confirmed by its oxygen isotopic composition (^{17}O = +1.90, ^{18}O = +4.79; R. Clayton, pers. communication). This winonaite is texturally unusual, with large poikilitic orthopyroxenes, and, moreover, it contains large grains of the amphibole fluoro-edenite (Floss et al. 2003). Here, we describe the mineralogy and petrology of HaH 193, with an emphasis on the origin of the fluoro-edenite and the thermal history of HaH 193.

Experimental methods

Two thin sections of HaH 193 were examined, both provided by A. Bischoff of the University of Münster. The thin section of HaH 193 studied at Washington University (designated as section A in the text) has a total area of about 2.5 cm^2. Mineral compositions (major elements) were determined using the Washington University JEOL JXA-733 electron microprobe. Fully focused beam analyses were carried out with an accelerating voltage of 15 kV and a beam current of 20 nA. X-ray matrix corrections were made using silicate mineral and oxide standards and a modified CITZAF routine (Armstrong 1988) incorporated into the electron microprobe software. A second section (section B) was examined at the Natural History Museum in London. This section has a total area of ~0.5 cm^2. Mineral compositions were acquired using a Cameca SX-50 electron microprobe. Operating conditions were similar to those of the JEOL JX-733, except that the accelerating voltage used was 20 kV.

* E-mail: floss@wustl.edu

0003-004X/07/0004–460$05.00/DOI: 10.2138/am.2007.2253

In addition, thin section A was mapped in a tiled pattern of 62 slightly overlapping areas using a JEOL 840a scanning electron microprobe (SEM) at 10 kV and 5 nA beam current. Each tiled area was imaged at 50× magnification in 1024^2 pixels for back-scattered electrons (BSE) and 256^2 pixels for X-ray elemental signals of Al, Ca, Fe, Mg, Na, P, Si, and S, resulting in a spatial resolution of ~7 µm/pixel for the elemental distribution images. The elemental maps were then processed using custom software, described below, to identify individual mineral phases and to determine the modal composition of the sample.

After manually identifying representative samples of all mineral phases of interest within the mapped area, the program was used to determine the range (maximum and minimum) of all elemental signals in those image pixels that are spatially correlated with the sample mineral phase. Typically only a few elements are diagnostic for the identification of a given mineral. The software then applies identification rules for each phase, based on the expected range of elemental signals, which are applied to the entire image by comparing elemental intensities at each pixel to those of the known mineral phases. An output image is created by coding each pixel with the predefined color of the matching mineral or by leaving it white when no match is found. Individual mineral identification rules can be adjusted manually to ensure correct identification of all phases. Successful rules from one tile of a larger map can be applied to all other tiles and the resulting output images are stitched together to create a mineral distribution mosaic (cf. Fig. 1). The relative contributions of each mineral type (i.e., pixel color) were used to determine the modal composition of the entire mapped section. It is difficult to assign a quantitative error to the modal determination, since it depends on a variety of factors, including image resolution, mineral grain size distribution, and the accuracy of the rules used to produce the mineral maps. However, the major source of uncertainty in the mode is likely to be due to the difficulty of determining exact phase boundaries, given the limited resolution of the X-ray maps.

Thin section B was also mapped, using a JEOL 5900 LV SEM at 20 kV and 2 nA beam current. The maps were imaged at 200× magnification for all available elements, and were automatically tiled using the Oxford Instruments INCA software package. Modal abundances of minerals were determined from this tiled image using Adobe Photoshop. Uncertainties in the modes are likely to be similar to those noted above for section A, and are probably also mainly due to the limited spatial resolution of the X-ray maps.

Concentrations of the rare-earth elements (REE) and other trace elements were determined using the modified Cameca ims 3f ion microprobe at Washington University, according to techniques described by Zinner and Crozaz (1986a). All analyses were made using an O^- primary beam and energy filtering at low mass resolution to remove complex molecular interferences. The resulting mass spectrum is deconvolved in the mass ranges K-Ca-Sc-Ti, Rb-Sr-Y-Zr, and Ba-REE to remove simple molecular interferences that are not eliminated with energy filtering (Alexander 1994; Hsu 1995). Sensitivity factors for the REE in pyroxene, amphibole, and Ca-phosphate are from Zinner and Crozaz (1986b) and for plagioclase are from Floss and Jolliff (1998). Sensitivity factors for other elements in the silicates are from Hsu (1995) and are listed in Table 1 of Floss et al. (1998). Absolute concentrations are determined using sensitivity factors relative to Si for the silicates and Ca for the phosphates. The CaO concentrations used for the phosphates (apatite) were determined from EDX analyses of the grains analyzed, whereas SiO_2 concentrations for the silicates are the averages of the values determined by electron microprobe. REE abundances in the figures are normalized to the CI abundances of Anders and Grevesse (1989).

Raman spectra were collected on a HoloLab 5000 spectrometer (Kaiser Optical Systems, Inc.) at Washington University. The 532 nm line from a frequency-doubled Nd:YAG laser was used as the excitation source, producing a condensed beam ~6 µm in diameter at the sample and a laser power of 10.5 mW at the sample surface. The spectral resolution of the spectrograph in the HoloLab 5000 system is 4–5 cm^{-1}. The wavelength calibration of the system uses a least squares curve-fitting procedure that compares the measured lines of a Ne lamp to standard values. The resulting wavelength accuracy is better than 0.003 nm in the region of interest, and is monitored for reproducibility daily using the Raman shift of a silicon wafer. All of the spectra were acquired using a 20× long-working-distance objective (0.4 NA) and spectral accumulation times of 40 seconds.

Results

Both sections of HaH 193 are dominated by very large (up to 5 mm), optically continuous orthopyroxene grains that poikilitically enclose smaller grains of olivine, plagioclase, and occasionally clinopyroxene (Fig. 1). Interstitial to the orthopyroxene poikiloblasts are clumps of equigranular 200–300 µm olivine grains, similar to areas described in Winona and other winonaites (Benedix et al. 1998), and large (up to 2 mm) grains of amphibole (identified as fluoro-edenite; see below) that are associated with, and locally poikilitically enclose, smaller grains of olivine, plagioclase and clinopyroxene (Fig. 2). Although some amphibole grains partially intrude into orthopyroxene, none of them is completely enclosed in these large poikilitic grains. Fe,Ni metal and troilite (which are not distinguished from each other in the composite map in Fig. 1) occur as clumps and veins throughout the sections. A vein of alteration material, probably of terrestrial origin, runs through the bottom third of section A (Fig. 1). Modally, HaH 193 is dominated by mafic silicate minerals (63–78 vol%, mainly orthopyroxene; Table 1), with lesser amounts of plagioclase (11 vol%) and trace apatite (0.2–0.3 vol%); the remainder consists mostly of Fe,Ni metal, troilite, and schreibersite, and their weathering products. The two sections studied here are modally similar, except for a notable difference in the abundance of olivine, which is twice as high in section B as in A; section B contains correspondingly less metal and sulfides (Table 1). The modal abundances in HaH 193 are similar to those in other winonaites, which typically contain 52–80 vol% mafic silicates, 7–14 vol% plagioclase, and 20–37 vol% metal and sulfides (Table 1; Benedix et al. 1998). Whereas section B of HaH 193 has a high abundance of olivine, similar to those seen in most winonaites, the lower abundance of olivine in HaH 193 section A is like that of the more-primitive (i.e., less-metamorphosed) NWA 1463 (Table 1).

Major-element compositions are uniform in both sections and are consistent with those seen in other winonaites (Table 2; Benedix et al. 1998). As in other winonaites, the mafic minerals in HaH 193 have reduced compositions that fall between those of enstatite and ordinary (H) chondrites (Brearley and Jones 1998), with olivine compositions of $Fa_{4.3–4.6}$, orthopyroxene compositions of $Wo_{1.7–2.0}Fs_{4.9–5.1}$, and clinopyroxene compositions of $Wo_{43.2–44.2}Fs_{1.3–2.2}$. The plagioclase in HaH 193 is oligoclase

Table 1. Modal abundances (vol%) of minerals in HaH 193 and other winonaites*

	HaH 193		NWA 1463	Mount Morris	Winona	Pontlyfni	Tierra Blanca
	section A	section B					
orthopyroxene	48.0	52.0	46.4	47.5	53.1	26.6	39.3
clinopyroxene	0.7	2.5	7.7	2.9	0.6	4.4	3.0
amphibole	4.1	4.1					
olivine	9.7	18.9	8.6	16.2	14.6	20.5	16.5
plagioclase	10.9	10.6	6.5	6.8	11.4	12.5	7.7
phosphate	0.1	0.3	0.7	0.1	0.4	trace	trace
opaque minerals†	26.7	11.6	30.6	26.5	20.0	36.1	33.6

* Modes for other winonaites are unpublished data from this laboratory.
† Includes FeNi metal, FeS, chromite, schreibersite, and weathering products.

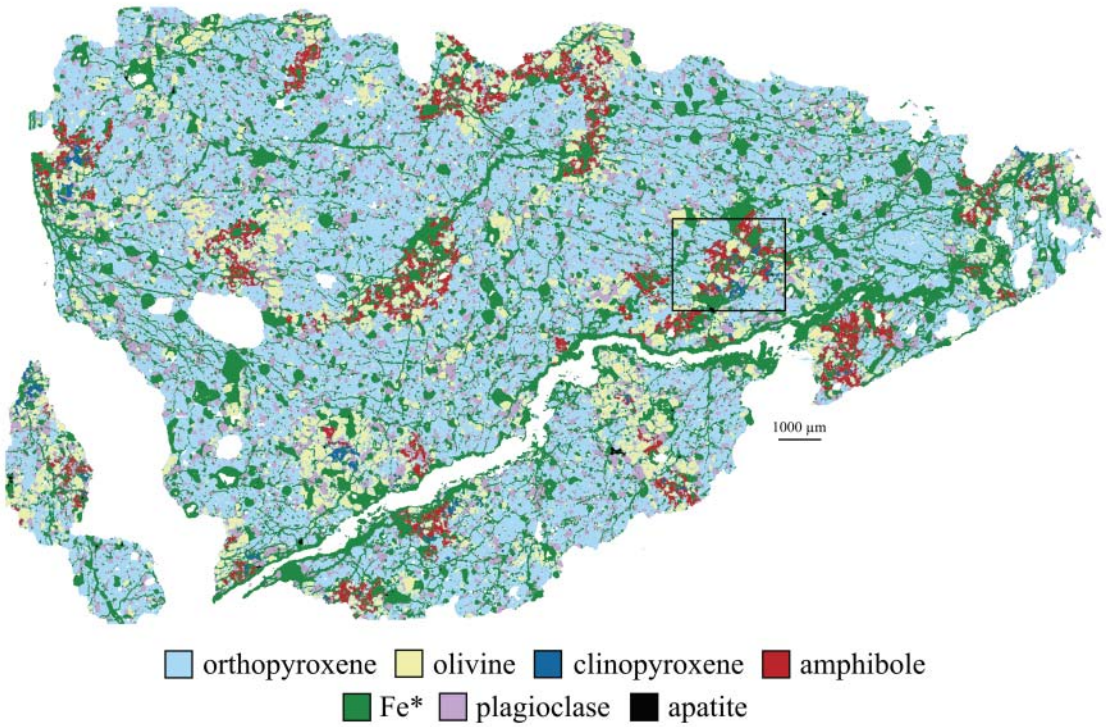

FIGURE 1. Elemental composite map of Hammadah al Hamra 193 (section A) showing the distribution of orthopyroxene, clinopyroxene, plagioclase, amphibole, olivine, apatite and Fe (Fe* refers to FeNi metal, as well as Fe-oxides, sulfides, and phosphides). White areas within the section are holes; a long vein filled with alteration material (of likely terrestrial origin) is also shown in white in the lower region of the section. The box indicates the amphibole-rich area shown in Figure 2.

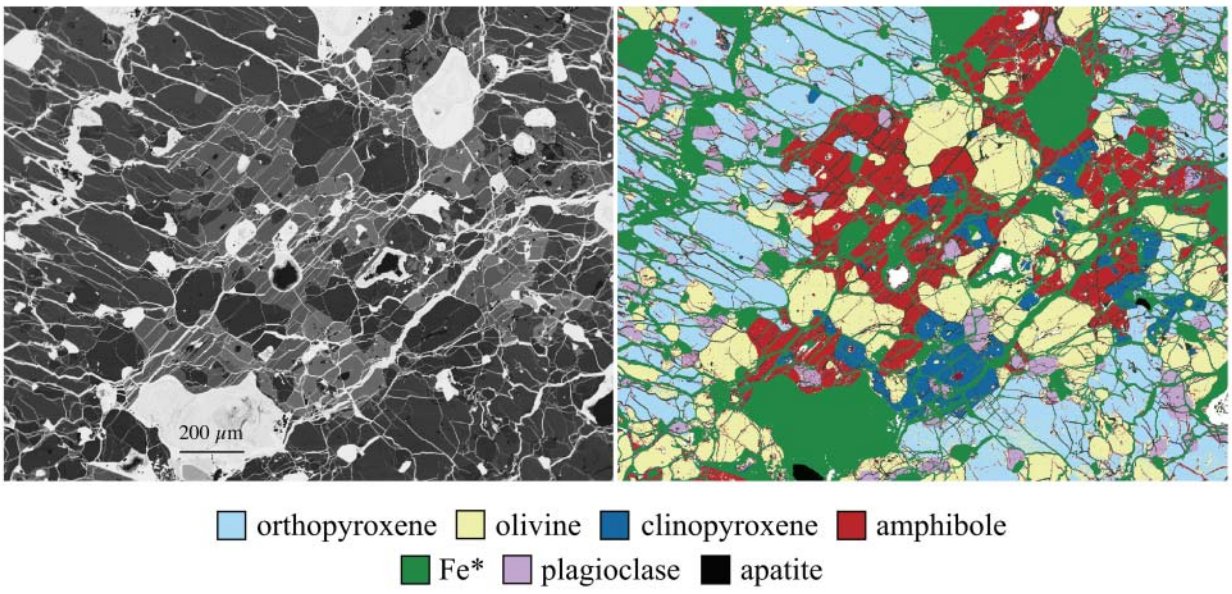

FIGURE 2. Detailed view of the amphibole-bearing lithology outlined in Figure 1. Left: back-scattered electron (BSE) image; right: element composite map. The amphibole is a single optically continuous grain situated between three large orthopyroxene poikiloblasts. White veins in the BSE image are terrestrial alteration.

TABLE 2. Major element compositions (wt%) of HaH 193 minerals*

	orthopyroxene		clinopyroxene		olivine		plagioclase		apatite	
	A	B	A	B	A	B	A	B	A	B
	n = 6	n = 6	n = 4	n = 23	n = 5	n = 10	n = 4	n = 6	n = 6	n = 3
SiO_2	58.6 (3)	58.5 (1)	54.9 (3)	54.9 (5)	41.5 (3)	42.1 (2)	61.9 (3)	62.7 (4)	0.04 (2)	n.d.
TiO_2	0.14 (5)	0.20 (5)	0.77 (2)	0.70 (12)	b.d.	b.d.	n.d.	0.04 (2)	n.d.	n.d.
Al_2O_3	0.28 (3)	0.29 (4)	0.67 (3)	0.68 (4)	b.d.	b.d.	23.3 (2)	22.0 (6)	b.d.	n.d.
Cr_2O_3	0.18 (5)	0.20 (3)	0.11 (7)	0.30 (25)	b.d.	0.03 (2)	n.d.	b.d.	n.d.	n.d.
FeO	3.24 (32)	3.64 (25)	1.04 (24)	1.26 (60)	4.41 (12)	4.52 (24)	0.19 (14)	0.27 (13)	0.49 (23)	0.40 (7)
MnO	0.26 (3)	0.32 (2)	0.08 (3)	0.15 (5)	0.22 (5)	0.31 (5)	n.d.	b.d.	0.05 (1)	n.d.
MgO	36.3 (2)	36.5 (4)	18.8 (2)	18.6 (4)	53.1 (4)	53.8 (5)	b.d.	b.d.	0.25 (1)	n.d.
CaO	0.96 (5)	1.36 (79)	22.5 (2)	22.5 (4)	b.d.	0.03 (1)	4.44 (8)	4.32 (46)	54.7 (5)	54.4 (8)
Na_2O	0.05 (2)	b.d.	0.48 (3)	0.52 (8)	b.d.	b.d.	8.92 (3)	9.13 (21)	b.d.	n.d.
K_2O	n.d.	b.d.	n.d.	b.d.	n.d.	b.d.	0.40 (3)	0.40 (4)	n.d.	n.d.
P_2O_5	n.d.	b.d.	n.d.	b.d.	n.d.	b.d.	n.d.	b.d.	42.3 (5)	41.8 (3)
F	n.d.	n.d.	n.d.	n.d.	n.d.	n.d.	n.d.	n.d.	3.44 (22)	3.38 (73)
Cl	n.d.	n.d.	n.d.	n.d.	n.d.	n.d.	n.d.	n.d.	0.55 (6)	0.71 (8)
Total	100.01	101.01	99.35	99.61	99.12		99.18	98.86	101.82	100.69
–O = F									1.45	1.42
–O = Cl									0.12	0.16
Total	100.0	101.0	99.4	99.6	99.2	100.8	99.2	98.9	100.3	99.1
HaH 193	$Wo_{1.7–2.0}Fs_{4.9–5.1}$		$Wo_{43.2–44.2}Fs_{1.3–2.2}$		$Fa_{4.3–4.6}$		$An_{20.9–21.4}$			
winonaites	$Wo_{1.5–2.0}Fs_{0.3–6.8}$		$Wo_{45.5–46.7}Fs_{0.4–2.7}$		$Fa_{0.3–5.3}$		$An_{7.7–25.1}$			

* Errors are 1 standard deviation; b.d. = below detection; n.d. = not determined.

TABLE 3. Major element compositions (wt%) of HaH 193 fluoro-edenite*

	fluoro-edenite			fluoro-edenite	
	A	B		A	B
	n = 6	n = 17	Cations		
SiO_2	49.7(4)	50.0(3)	Si	7.04	6.97
TiO_2	0.63(7)	1.08(22)	Ti	0.07	0.11
Al_2O_3	5.89(20)	5.88(23)	Al	0.98	0.97
Cr_2O_3	0.38(8)	0.62(11)	Cr	0.04	0.06
FeO	1.08(8)	1.25(17)	Fe	0.13	0.15
MnO	0.08(6)	0.09(2)	Mn	0.01	0.01
MgO	22.8(1)	23.3(2)	Mg	4.81	4.85
CaO	11.4(1)	11.2(1)	Ca	1.73	1.68
Na_2O	3.88(8)	4.09(12)	Na	0.07	1.11
K_2O	0.45(1)	0.48(3)	K	0.08	0.09
P_2O_5	n.d.	b.d.	P	n.d.	b.d.
F	4.05(1)	4.56(13)	F	1.82	2.01
Cl	0.04(1)	n.d.	Cl	0.01	n.d.
Total	100.38	102.55	Total	17.78	18.01
–O = F	1.71	1.92			
–O = Cl	0.01				
Total	98.7	100.6			

* Errors are 1 standard deviation; b.d. = below detection; n.d. = not determined.

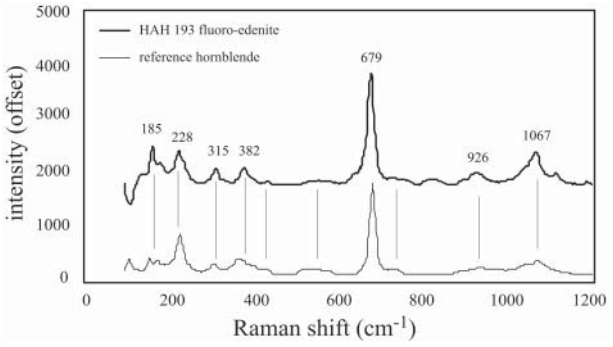

FIGURE 3. Raman spectrum of HaH 193 fluoro-edenite compared to the Raman spectrum of an amphibole (ASU WAR0392 hornblende). Vertical lines show corresponding features other than the main Si-bridging-oxygen vibrational peak at ~679 cm^{-1}. The spectrum of HaH 193 amphibole has no peaks in the OH region ~3600–3800 cm^{-1} (not shown), consistent with its high F content.

($An_{20.9–21.4}$) and falls within the range of compositions observed in other winonaites (Table 2; Benedix et al. 1998). Apatite in HaH 193 is fluor-apatite, with 3.4 wt% F (Table 2). Analyses of amphibole in HaH 193 (Table 3) show that it is nearly stoichiometric fluoro-edenite, with a formula of:

$$K_{0.08–0.09}Na_{0.07–1.1}Ca_{1.68–1.73}Mg_{4.81–4.85}Fe_{0.13–0.15}Si_{6.97–7.04}Al_{0.97–0.98}O_{22}F_{1.82–2.01}$$

We used Raman spectroscopy to confirm the amphibole structure of this phase. Figure 3 shows the Raman spectrum of HaH 193 fluoro-edenite compared to the spectrum of hornblende WAR0392 from Arizona State University. In addition to the main Si–bridging-oxygen vibrational peak at 679 cm^{-1}, numerous other corresponding features (shown by the vertical lines) indicate a match with the amphibole structure. The spectrum of the HaH 193 amphibole, moreover, shows no peak in the OH region at ~3600–3800 cm^{-1}, consistent with the high measured F content.

The silicate phases in HaH 193 each have uniform REE compositions (Table 4; Fig. 4), consistent with their homogeneous major-element compositions. Orthopyroxene REE compositions are enriched in the heavy (H)REE, and the REE pattern has a negative Eu anomaly, whereas plagioclase is light (L)REE-enriched with a positive Eu anomaly. Clinopyroxene and amphibole have similar bow-shaped REE patterns that are enriched in the middle (M)REE with negative Eu anomalies. Phosphate patterns are more variable: all are relatively flat with negative Eu anomalies, but apatite 1 has REE abundances of ~40 × CI, about a factor of two lower than the other two apatite grains measured.

DISCUSSION

Bulk REE composition and winonaite sample heterogeneity

We used the REE compositions measured here (Table 4) and the modal abundances of HaH 193 to determine the bulk REE composition of this meteorite (Fig. 5). The REE pattern calculated using the mode from section A is slightly LREE-enriched

TABLE 4. Minor and trace element compositions (ppm) of HaH 193 minerals determined by SIMS*

	average orthopyroxene n = 5	average clinopyroxene n = 5	average fluoro-edenite n = 5	average olivine n = 2	average plagioclase n = 3	apatite 1 n = 1	apatite 2 n = 1	apatite 3 n = 1
F	47(13)	395(40)	50000(3000)	76(9)	9.0(3.4)	41600(250)	40150(240)	39050(280)
Na	220(60)	2670(220)	22100(900)	19(5)	71000(700)	n.d.	n.d.	n.d.
P	15(18)	16(9)	25(10)	7(3)	7.3(6)	n.d.	n.d.	n.d.
K	5(7)	24(17)	2770(110)	1.2(6)	2960(100)	n.d.	n.d.	n.d.
Sc	7.6(7)	72(2)	53(3)	1.9(8)	1.5(1)	n.d.	n.d.	n.d.
Ti	550(65)	3370(320)	2930(250)	21(2)	145(20)	n.d.	n.d.	n.d.
V	19(5)	51(4)	95(16)	10(1)	5.3(3)	n.d.	n.d.	n.d.
Mn	1450(290)	955(105)	590(70)	1590(110)	n.d.	n.d.	n.d.	n.d.
Sr	0.057(27)	6(2)	7(1)	0.048(33)	91(3)	n.d.	n.d.	n.d.
Y	1.4(1)	28(2)	17(2)	0.006(1)	0.064(6)	n.d.	n.d.	n.d.
Zr	0.96(19)	83(13)	85(32)	0.056(18)	0.22(2)	n.d.	n.d.	n.d.
Ba	0.012(15)	0.087(99)	1.5(3)	0.004(3)	14(1)	n.d.	n.d.	n.d.
La	b.d.	1.5(4)	0.89(17)	b.d.	0.71(13)	7.1(4)	19(1)	17(1)
Ce	b.d.	5.4(6)	3.2(6)	b.d.	1.0(3)	20(1)	50(2)	48(2)
Pr	b.d.	1.0(1)	0.60(7)	b.d.	0.072(17)	2.9(2)	5.9(4)	6.5(4)
Nd	0.019(6)	5.4(6)	2.9(3)	b.d.	0.19(4)	17(1)	30(1)	33(1)
Sm	0.014(2)	1.9(1)	1.1(2)	b.d.	0.025(7)	6.2(5)	9.8(6)	11(1)
Eu	0.0002(3)	0.007(6)	0.026(6)	b.d.	0.40(9)	0.69(7)	1.1(1)	0.82(8)
Gd	0.028(6)	2.5(2)	1.6(5)	b.d.	0.015(7)	8.0(7)	14(1)	14(1)
Tb	0.007(2)	0.44(8)	0.29(11)	b.d.	b.d.	1.7(1)	3.1(2)	3.0(3)
Dy	0.054(12)	2.5(3)	1.5(4)	b.d.	0.012(3)	9.7(5)	21(1)	18(1)
Ho	0.013(6)	0.44(4)	0.24(7)	b.d.	b.d.	2.4(2)	4.9(3)	3.9(3)
Er	0.055(14)	1.1(1)	0.63(19)	b.d.	b.d.	5.5(3)	15(1)	13(1)
Tm	0.008(2)	0.14(3)	0.073(29)	b.d.	b.d.	0.70(8)	2.6(2)	1.7(2)
Yb	0.058(10)	0.77(16)	0.32(7)	b.d.	0.003(2)	5.2(3)	19(1)	13(1)
Lu	0.010(2)	0.089(15)	0.041(24)	b.d.	b.d.	0.59(9)	2.1(2)	2.1(3)

* Errors are 1 standard deviation for averages or 1 due to counting statistics; all measurements made on section A. b.d. = below detection; n.d. = not determined.

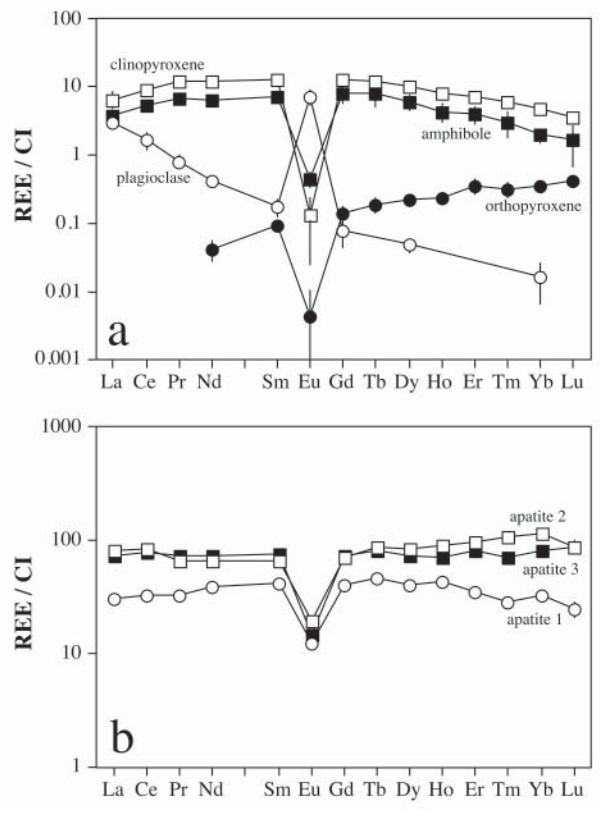

FIGURE 4. CI chondrite-normalized REE patterns for (**a**) silicates and (**b**) phosphates from HaH 193. Errors are 1 standard deviations for the average compositions of the silicates and 1 counting statistics errors for the phosphates (and are smaller than the symbol sizes for many of the REE).

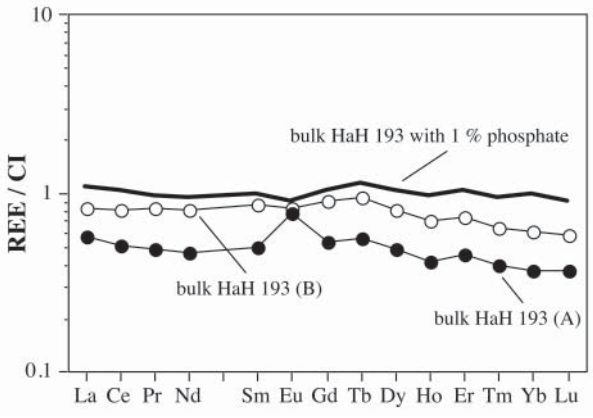

FIGURE 5. CI chondrite-normalized REE patterns for bulk HaH 193, as reconstructed from mineral compositions and modal abundances (filled circles). The line shows the calculated bulk REE pattern assuming a higher modal abundance of phosphate. (See text for details.)

with sub-chondritic abundances (La = ~0.6 × CI; Lu = ~0.4 × CI) and has a small positive Eu anomaly, whereas the REE pattern calculated from mode B is approximately flat with higher abundances of ~0.8 × CI. Phosphate is the only mineral in this meteorite that shows variable REE abundances (Table 4; Fig. 4) and, as trace minerals, phosphates are heterogeneously distributed in many meteorites. The sub-chondritic REE pattern calculated from our data could, therefore, be due to inadequate sampling of phosphate in our section, either in terms of the range of REE compositions, or, more likely, in terms of a representative modal abundance for HaH 193. We note that an increase in the modal abundance of phosphate to 1.0 vol% results in a bulk REE pattern that is flat with chondritic abundances and no anomalies (Fig. 5).

Most of the whole-rock REE data obtained to date on winonaites (e.g., Davis et al. 1977; Prinz et al. 1980; Kallemeyn and Wasson 1985; Yamamoto et al. 1991; Kimura et al. 1992) have shown considerable variability, both between and within individual meteorites. For example, Prinz et al. (1980) found that two splits of Winona have complementary REE patterns: one split has a relatively flat REE pattern with a negative Eu anomaly, whereas the REE pattern for the other split is V-shaped with a large positive Eu anomaly. Although it has been argued that these fractionated REE patterns indicate igneous differentiation processes occurring on the winonaite parent body (Davis et al. 1977; Prinz et al. 1980), it is more likely that the variability is due to heterogeneous sampling of minor REE-bearing phases as well as of major mineral phases. This conclusion is supported by the fact that many of the fractionated REE patterns observed are V-shaped with enrichments of both the light and heavy REE, a feature that cannot be produced by an appropriate igneous-fractionation process, but that can readily be accounted for by a mixture of minerals with light and heavy REE enrichments, such as plagioclase and pyroxene. Benedix et al. (1998) noted that, despite their equigranular textures, some winonaites contain regions with substantially different grain sizes and/or mineralogies, as discussed above, and preferential sampling of such areas, as well as heterogeneous distribution of phosphate, the major REE carrier, probably accounts for the non-chondritic patterns observed.

Formation of fluoro-edenite in HaH 193

Amphiboles are rare in meteorites and are most commonly found as micrometer-sized grains in magmatic inclusions trapped in mafic silicate grains in Martian meteorites. The type of amphibole reported in these meteorites is kaersutite, characterized by high contents of Ca, Al, and Ti (Mikouchi and Miyamoto 2000 and references therein). In addition, several occurrences are reported from asteroidal meteorites. Kaersutite has been reported from the ungrouped iron meteorite Sombrerete (Prinz et al. 1982), and fluor-richterite has been reported from the IAB irons Wichita County and Canyon Diablo (Olsen 1967; Olsen et al. 1973), the enstatite chondrite Abee (Douglas and Plant 1968) and the enstatite achondrite Mayo Belwa (Bevan et al. 1977). Brearley (1997) also reported the presence of calcic amphibole with a composition close to that of magnesiohornblende from the carbonaceous chondrite Allende.

Fluoro-edenite is an uncommon amphibole (Leake et al. 1997) that has only recently been identified terrestrially (Gianfagna and Oberti 2001). In the one natural terrestrial occurrence that has been reported, fluoro-edenite is present as millimeter-sized crystals in altered benmoreitic lavas, associated with feldspars, quartz, and clino- and orthopyroxenes, and probably crystallized from late-stage hydrothermal fluids with high F contents (Gianfagna and Oberti 2001). Ours is the first reported meteoritic occurrence. The textures in HaH 193 suggest that the fluoro-edenite is replacing clinopyroxene, probably in a reaction between clinopyroxene and plagioclase such as:

$$\underset{\text{diopside}}{MgCaSi_2O_6} + \underset{\text{plagioclase}}{NaAlSi_3O_8} + \underset{\text{olivine}}{2Mg_2SiO_4} + CaF_2 = \underset{\text{fluoro-edenite}}{NaCa_2Mg_5AlSi_7O_{22}F_2}$$

Trace-element data support the formation of fluoro-edenite by a reaction similar to the one given above. Clinopyroxene and fluoro-edenite have similar bow-shaped REE patterns with negative Eu anomalies (Fig. 4). However, relative to clinopyroxene, the fluoro-edenite has lower trivalent REE abundances by a factor of two and higher abundances of Eu by a factor of three, consistent with the contribution of plagioclase (with high Eu contents) to the formation of the amphibole. The fluoro-edenite also has elevated abundances of other elements commonly enriched in plagioclase, such as Na (~10×), K (~100×), and Ba (~15×), relative to clinopyroxene, but has virtually identical abundances of elements commonly found in pyroxene, such as Sc, Ti, Mn, Y, and Zr (Fig. 6). In addition, because it is the only source for Na, this reaction would tend to make plagioclase more calcic and, indeed, plagioclase compositions in HaH 193 are at the high-Ca end of the range observed for other winonaites (Table 2).

The source of the F for the formation of fluoro-edenite in HaH 193 is somewhat uncertain. The most straightforward explanation is it comes from a fluid enriched in both Ca and F, derived from the breakdown of phosphate, which is fluor-apatite in HaH 193 (Table 2). However, there is clearly not enough fluor-apatite in HaH 193 to produce the large amount of fluoro-edenite present, even if one assumes that HaH 193 initially contained the modal abundance of 1 vol% required to provide chondritic bulk REE abundances, as discussed above. Moreover, other winonaites do not contain significantly more phosphate (Table 1), and many contain chlor-apatite or merrillite rather than the fluor-apatite found in HaH 193. Another possibility is that the F originates from a secondary source, such as the presence of a metasomatizing fluid during metamorphism. Fluor-apatite could then be an additional product of the same fluorination reaction that produced the fluoro-edenite.

It has been suggested that the scarcity of amphiboles with edenite compositions may be due to a structural instability (Raudsepp et al. 1991). These authors found that low-pressure synthesis experiments produced only minimal amounts of edenite. Although fluoro-edenite appears to be more easily synthesized, non-stoichiometric compositions are common (Graham and Navrotsky 1986; Raudsepp et al. 1991; Oberti et al. 1998). Moreover, studies of edenite phase relations to 3 kbar (Na et al. 1986) indicate no substantial equilibrium solid solution toward

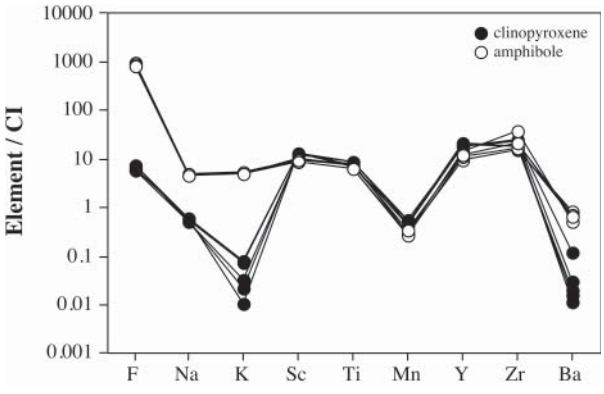

FIGURE 6. CI chondrite-normalized abundances of trace elements in individual grains of clinopyroxene and amphibole from HaH 193.

edenite compositions in SiO_2-excess systems and stability only over a very limited temperature range in SiO_2-undersaturated systems, thus accounting for the rarity of this mineral in nature. However, our observation of substantial amounts of end-member fluoro-edenite in HaH 193 show that there is in fact a definite stability field for fluoro-edenite. It may be that very Mg-rich compositions are required to stabilize this mineral. Gianfagna and Oberti (2001) observed the presence of substantial Mg at the M4' site, indicating a disordered distribution of medium-size divalent cations in their terrestrial fluoro-edenite. Although they noted that this could be a consequence of high-temperature crystallization combined with rapid quenching, they also suggest a crystal-chemical explanation that would promote stability of this composition. The smaller Mg cations at the M4' site allow kinking of the double chain of tetrahedra, thus reducing the chain repeat distance along the **c** axis and promoting matching with the octahedral strips, particularly when there is nearly complete Mg occupancy of the site (Gianfagna and Oberti 2001). The Mg-rich mineral compositions in HaH 193, and the fact that fluoro-edenite in HaH 193 formed under conditions of extended metamorphism (see below), suggest that this explanation is correct and does confer enhanced stability of this mineral.

Metamorphism on the winonaite parent body

As noted above, most winonaites are relatively fine- to medium-grained with well-developed, equigranular textures, indicative of the metamorphism they have undergone. Benedix et al. (1998) noted that winonaites show a range of two-pyroxene equilibration temperatures from 730 to 1200 °C (although uncertainties are relatively large, ~100 °C). These equilibration temperatures generally correlate with the grain sizes of the meteorites; thus, Pontlyfni, which is one of the most fine-grained winonaites, has a relatively low equilibration temperature of 975 °C, whereas Tierra Blanca, with the largest average grain size, has the highest equilibration temperature. Tierra Blanca also contains large poikilitic grains of clinopyroxene (up to 9 mm in size; King et al. 1981), enclosing olivine, plagioclase, and orthopyroxene grains. King et al. (1981) and Benedix et al. (1998) have argued that these large poikilitic clinopyroxenes formed by solid-state metamorphism rather than through crystallization from a melt; growth of such poikilitic pyroxenes is also well known from terrestrial metamorphic rocks (e.g., Kretz 1994). In contrast to other winonaites that are dominated by equigranular textures with abundant 120° triple junctions (including most portions of Tierra Blanca), our section of HaH 193 consists primarily of large poikilitic orthopyroxene and amphibole grains, that enclose smaller grains of plagioclase, olivine, and clinopyroxene. These grains most likely also formed through solid-state metamorphism and indicate that this meteorite is considerably more equilibrated than other winonaites. The homogeneity of mineral compositions, for both major elements (Tables 2 and 3) and trace elements (Table 4), is also consistent with a high degree of equilibration. Determination of the two-pyroxene equilibration temperature based on Ca-exchange (Kretz 1982) yields a temperature of ~1000 °C for HaH 193, which is somewhat lower than that determined for Tierra Blanca, the only other winonaite known to contain such poikilitic grains. However, it is interesting to note that HaH 193 also appears to have an Fe-Mg exchange equilibration temperature (Kretz 1982) of 1000 °C, indicating that it is completely equilibrated. HaH 193 and Tierra Blanca, which both have large poikiloblasts, may have spent a longer time at metamorphic temperatures than other winonaites that have equigranular textures. The presence of fluoro-edenite in HaH 193 also provides some constraints. Fluoro-edenite has been synthesized at low pressures (up to 2 kbar) and temperatures ranging from ~800–1200 °C (Graham and Navrotsky 1986; Raudsepp et al. 1991; Oberti et al. 1998), consistent with the equilibration temperatures calculated for HaH 193. Moreover, the fact that fluoro-edenite can be synthesized at low pressures is consistent with its formation on a relatively small asteroid, such as the winonaite/IAB parent body.

Benedix et al. (1998, 2000) noted that the winonaite/IAB parent body experienced variable degrees of heating, with peak temperatures above those at which silicate partial melting occurs. Evidence for heterogeneous heating is preserved in these meteorites on a local scale, as evidenced by their variable textures, sometimes within a single thin section, and the lack of a correlation between the olivine–chromite and the two-pyroxene geothermometers (Benedix et al. 2005). These authors argued that the variable heating noted in these meteorites is consistent with catastrophic breakup and reassembly of the winonaite/IAB parent body after peak temperatures were reached, with different parts of the parent body experiencing a range of reheating and cooling histories over short distances. The extensive thermal metamorphism experienced by HaH 193 indicates that it must have experienced slow cooling for an extended time period, which probably occurred at depth in the winonaite/IAB parent body. Growth of the large poikilitic orthopyroxene grains, as well as the formation of fluoro-edenite, most probably occurred during this final metamorphic episode.

Acknowledgments

We thank John Spratt (NHM) for help on the electron microprobe, and Tim Smolar and Eric Inazaki (WU) for maintenance of the 3f ion microprobe. We also gratefully acknowledge careful reviews by A. Gianfagna, M. Kimura, and R. Jones, which helped to significantly improve this paper. This research was supported by NASA grant NNG04GG49G to C.F.

References cited

Alexander, C.M.OD (1994) Trace element distributions within ordinary chondrite chondrules: implications for chondrule formation conditions and precursors. Geochimica et Cosmochimica Acta, 58, 3451–3467.

Anders, E. and Grevesse, N. (1989) Abundances of the elements: meteoritic and solar. Geochimica et Cosmochimica Acta, 53, 197–214.

Armstrong, J.T. (1988) Quantitative analysis of silicate and oxide materials: comparison of Monte Carlo, ZAF and (,z) procedures. Microbeam Analysis, 23, 239–245.

Benedix, G.K., McCoy, T.J., Keil, K., Bogard, D.D., and Garrison, D.H. (1998) A petrologic and isotopic study of winonaites: evidence for early partial melting, brecciation, and metamorphism. Geochimica et Cosmochimica Acta, 62, 2535–2553.

Benedix, G.K., McCoy, T.J., Keil, K., and Love, S.G. (2000) A petrologic study of the IAB iron meteorites: constraints on the formation of the IAB-winonaite parent body. Meteoritics and Planetary Science, 35, 1127–1141.

Benedix, G.K., McCoy, T.J., and Lauretta, D.S. (2003) Is NWA 1463 the most primitive winonaite? Meteoritics and Planetary Science, 38, A70.

Benedix, G.K., Lauretta, D.S., and McCoy, T.J. (2005) Thermodynamic constraints on the formation conditions of winonaites and silicate-bearing IAB irons. Geochimica et Cosmochimica Acta, 69, 5123–5131.

Bevan, A.W.R., Bevan, J.C., and Francis, J.G. (1977) Amphibole in the Mayo Belwa meteorite: first occurrence in an enstatite achondrite. Mineralogical Magazine, 41, 531–534.

Brearley, A. (1997) Disordered biopyriboles, amphibole, and talc in the Allende meteorite: products of nebular or parent body aqueous alteration. Science,

276, 1103–1105.
Brearley, A.J. and Jones, R.H. (1998) Chondritic Meteorites. In J.J. Papike, Ed., Planetary Materials, 36, p. 3-1–3-398. Reviews in Mineralogy, Mineralogical Society of America, Chantilly, Virginia.
Clayton, R.N. and Mayeda, T.K. (1996) Oxygen isotope studies of achondrites. Geochimica et Cosmochimica Acta, 60, 1999–2017.
Davis, A.M., Ganapathy, R., and Grossman, L. (1977) Pontlyfni: a differentiated meteorite related to the Group IAB irons. Earth and Planetary Science Letters, 35, 19–24.
Douglas, J.A.V. and Plant, A.G. (1968) Amphibole: first occurrence in an enstatite chondrite. Meteoritics, 4, 166.
Floss, C. (2000) Complexities on the acapulcoite-lodranite parent body: evidence from trace element distributions in silicate minerals. Meteoritics and Planetary Science, 35, 1073–1085.
Floss, C. and Jolliff, B. (1998) Rare earth element sensitivity factors in calcic plagioclase (anorthite). In G. Gillen, R. Lareau, J. Bennett, and F. Stevie, Eds., Secondary Ion Mass Spectrometry, SIMS XI, p. 785–788. John Wiley and Sons, New York.
Floss, C., James, O.B., McGee, J.J., and Crozaz, G. (1998) Lunar ferroan anorthosite petrogenesis: clues from trace element distributions in FAN subgroups. Geochimica et Cosmochimica Acta, 62, 1255–1283.
Floss, C., Jolliff, B., Reid, J., and Benedix, G. (2003) Hammadah al Hamra 193: an amphibole-bearing winonaite. Meteoritics and Planetary Science, 38, A22.
Gianfagna, A. and Oberti, R. (2001) Fluoro-edenite from Biancavilla (Catania, Sicily, Italy): crystal chemistry of a new amphibole end-member. American Mineralogist, 86, 1489–1493.
Graham, C.M. and Navrotsky, A. (1986) Thermochemistry of the tremolite-edenite amphiboles using fluorine analogues, and applications to amphibole-plagioclase-quartz equilibria. Contributions to Mineralogy and Petrology, 93, 18–32.
Grossman, J.N. (1998) The Meteoritical Bulletin, No. 82, 1998 July. Meteoritics and Planetary Science, 33, A221–A239.
Hsu, W. (1995) Ion microprobe studies of the petrogenesis of enstatite chondrites and eucrites, 380 p. Ph.D. thesis, Washington University.
Kallemeyn, G.W. and Wasson, J.T. (1985) The compositional classification of chondrites: IV. Ungrouped chondritic meteorites and clasts. Geochimica et Cosmochimica Acta, 49, 261–270.
Kimura, M., Tsuchiyama, A., Fukuoka, T., and Imura, Y. (1992) Antarctic primitive achondrites, Yamato-74025, -75300, and -75305: their mineralogy, thermal history, and the relevance to winonaite. Proceedings of the NIPR Symposium on Antarctic Meteorites, 5, 165–190.
King, E.A., Jarosewich, E., and Daugherty, F.W. (1981) Tierra Blanca: an unusual achondrite from West Texas. Meteoritics, 16, 229–237.
Kretz, R. (1982) Transfer and exchange equilibria in a portion of the pyroxene quadrilateral as deduced from natural and experimental data. Geochimica et Cosmochimica Acta, 46, 411–421.
——— (1994) Metamorphic crystallization, 530 p. Wiley and Sons, Inc., New York.
Leake, B.E., Woolley, A.R., Arps, C.E.S., Birch, W.D., Gilbert, M.C., Grice, J.D., Hawthorne, F.C., Kato, A., Kisch, H.J., Krivovichev, V.G., Linthout, K., Laird, J., Mandarino, J.A., Maresch, W.V., Nickel, E.H., Rock, N.M.S., Schumacher, J.C., Smith, D.C., Stephenson, N.C.N., Ungaretti, L., Whittaker, E.J.W., and Youzhi, G. (1997) Nomenclature of amphiboles: report of the subcommittee on amphiboles of the international mineralogical association, commission on new minerals and mineral names. Canadian Mineralogist, 35, 219–246.
McCoy, T.J., Keil, K., Clayton, R.N., Mayeda, T.K., Bogard, D.D., Garrison, D.H., Huss, G.R., Hutcheon, I.D., and Wieler, R. (1996) A petrologic, chemical, and isotopic study of Monument Draw and comparison with other acapulcoites: evidence for formation by incipient partial melting. Geochimica et Cosmochimica Acta, 60, 2681–2708.
McCoy, T.J., Keil, K., Clayton, R.N., Mayeda, T.K., Bogard, D.D., Garrison, D.H., and Wieler, R. (1997) A petrologic and isotopic study of lodranites: evidence for early formation as partial melt residues from heterogeneous precursors. Geochimica et Cosmochimica Acta, 61, 623–637.
Mikouchi, T. and Miyamoto, M. (2000) Micro Raman spectroscopy of amphiboles and pyroxenes in the martian meteorites Zagami and Lewis Cliff 88516. Meteoritics and Planetary Science, 35, 155–159.
Na, K.C., McCauley, M.L., Crisp, J.A., and Ernst, W.G. (1986) Phase relations to 3 kbar in the systems edenite + H_2O and edenite + excess quartz + H_2O. Lithos, 19, 153–163.
Oberti, R., Hawthorne, F.C., Camara, F., and Raudsepp, M. (1998) Synthetic fluoro-amphiboles: site preferences of Al, Ga, Sc and inductive effects on mean bond-lengths of octahedra. Canadian Mineralogist, 36, 1245–1252.
Olsen, E. (1967) Amphibole: first occurrence in a meteorite. Science, 156, 61–62.
Olsen, E., Huebner, J.S., Douglas, J.A.V., and Plant, A.G. (1973) Meteoritic amphiboles. American Mineralogist, 58, 869–872.
Prinz, M., Waggoner, D.G., and Hamilton, P.J. (1980) Winonaites: a primitive achondritic group related to silicate inclusions in IAB irons. Lunar and Planetary Science, XI, 902–904.
Prinz, M., Nehru, C.E., and Delaney, J.S. (1982) Sombrerete, an iron with highly fractionated amphibole-bearing Na-P-rich silicate inclusions. Lunar and Planetary Science, XIII, 634–635.
Raudsepp, M., Turnock, A.C., and Hawthorne, F.C. (1991) Amphibole synthesis at low pressure: what grows and what doesn't. European Journal of Mineralogy, 3, 983–1004.
Yamamoto, K., Nakamura, N., Misawa, K., Yanai, K., and Matsumoto, Y. (1991) Lithophile trace element abundances in Antarctic unique meteorites and in unique clasts from L6 chondrites. Symposium on Antarctic Meteorites, 15, 97–98.
Zinner, E. and Crozaz, G. (1986a) A method for the quantitative measurement of rare earth elements by ion microprobe. International Journal of Mass Spectrometry and Ion Processes, 69, 17–38.
——— (1986b) Ion probe determination of the abundances of all the rare earth elements in single mineral grains. In A. Benninghoven, R.J. Colton, D.S. Simons, and H.W. Werner, Eds., Secondary Ion Mass Spectrometry, SIMS V, p. 444–446. Springer-Verlag, Berlin.

Manuscript received March 2, 2006
Manuscript accepted October 11, 2006
Manuscript handled by Rhian Jones